Supporting Information

Nanoenabled Disruption of Multiple Barriers in Antigen Cross-Presentation of Dendritic Cells *via* Calcium Interference for Enhanced Chemo-Immunotherapy

Jingyi An[†], Kaixiang Zhang[†], Binghua Wang[†], Sixuan Wu[†], Yifei Wang[†], Hongling Zhang[†], Zhenzhong Zhang[†,*], Junjie Liu[†,*] and Jinjin Shi[†,*]

[†]School of Pharmaceutical Sciences, Zhengzhou University, Zhengzhou 450001, China

*E-mail: zhangzhenzhong@zzu.edu.cn; liujunjie@zzu.edu.cn; shijinyxy@zzu.edu.cn

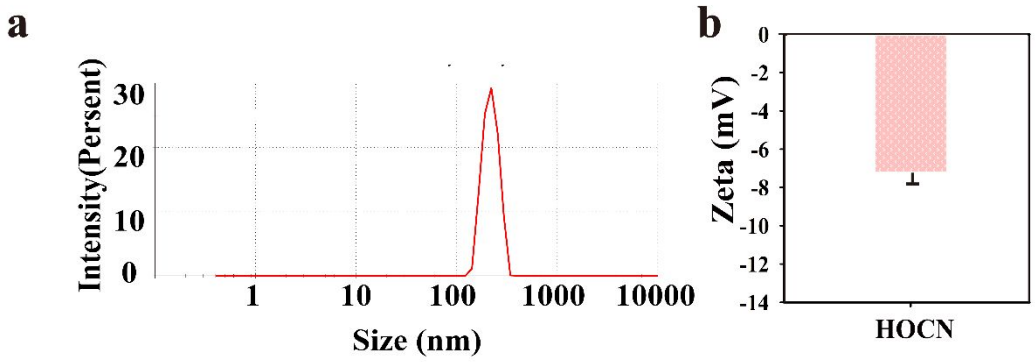

Fig. S1 Size distribution (A) and zeta potential (B) of HOCN. Results are presented as means ± s.d., n=4, **P* < 0.05, ***P* < 0.01, and ****P* < 0.001 determined by Student's t test.

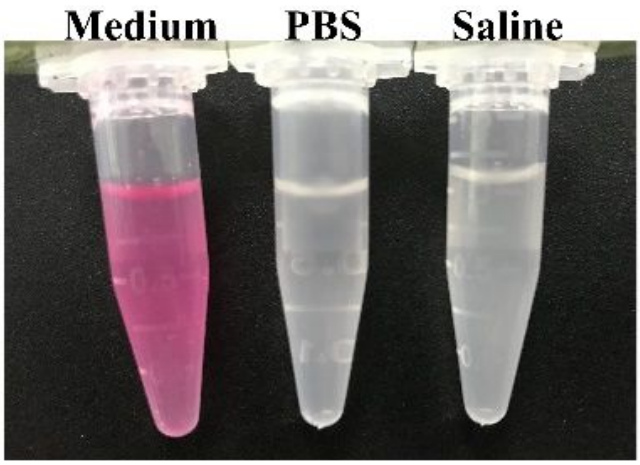

Fig. S2 Photos of HOCN in cell medium, PBS (pH 7.4) and saline for 1 weeks.

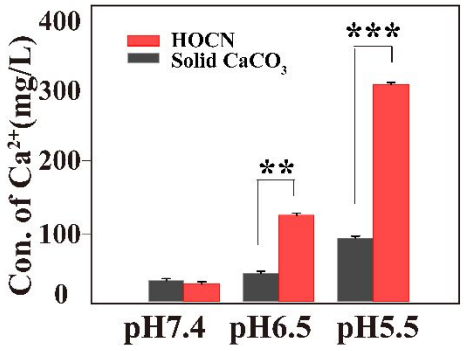

Fig. S3 The corresponding concentrations of Ca^{2+} in supernatant after incubation in PBS with different pH values (5.5, 6.5 and 7.4) for 24 h. Results are presented as means ± s.d., n=4, *$P < 0.05$, **$P < 0.01$, and ***$P < 0.001$ determined by Student's t test.

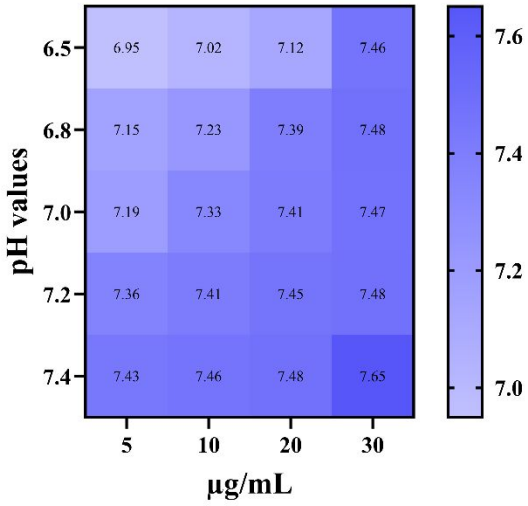

Fig. S4 The corresponding pH values of cell medium after incubation with different concentration of HOCN (5, 10, 20 and 30 μg/mL) with different initial pH values for 3 h.

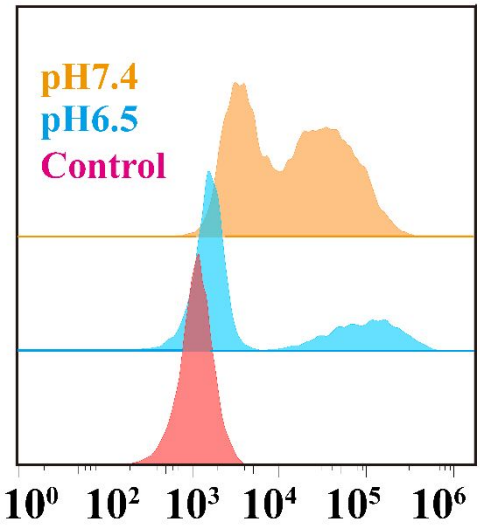

Fig. S5 Cellular uptake efficiency of DCs to HOCN@FITC after incubation in different pH values of cell medium for 24 h.

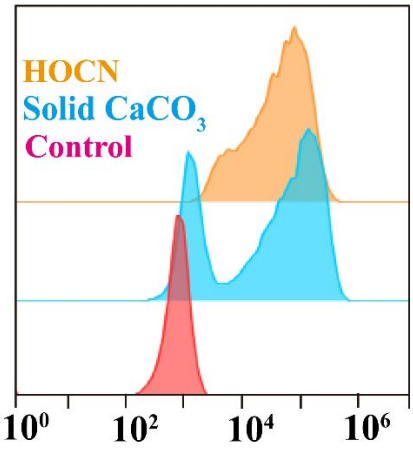

Fig. S6 The cellular uptake efficiency of DCs treated with HOCN and solid $CaCO_3$ for 1 h, and the nanoparticles were labeled with FITC.

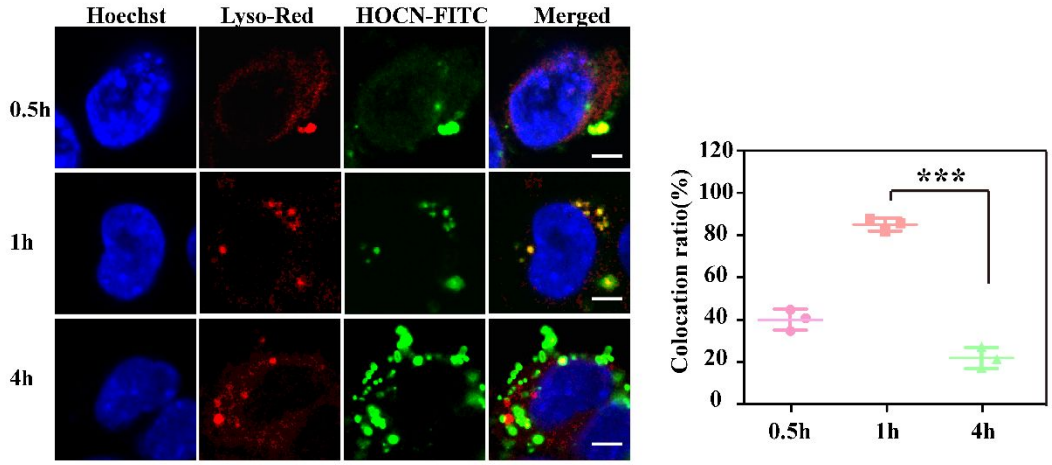

Fig. S7 The CLSM and co-location ratio of HOCN with lysosomes in DCs after incubation with HOCN for 0.5, 1 and 4 h, respectively. Results are presented as means ± s.d., n=3, **P* < 0.05, ***P* < 0.01, and ****P* < 0.001 determined by Student's t test.

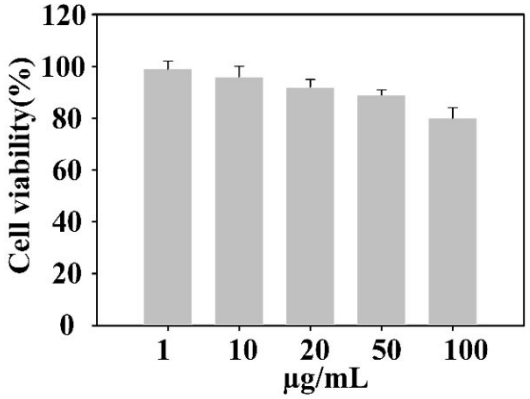

Fig. S8 The cell viability of DCs treated with different concentrations of HOCN for 24 h. Results are presented as means ± s.d., n=6, **P* < 0.05, ***P* < 0.01, and ****P* < 0.001 determined by Student's t test.

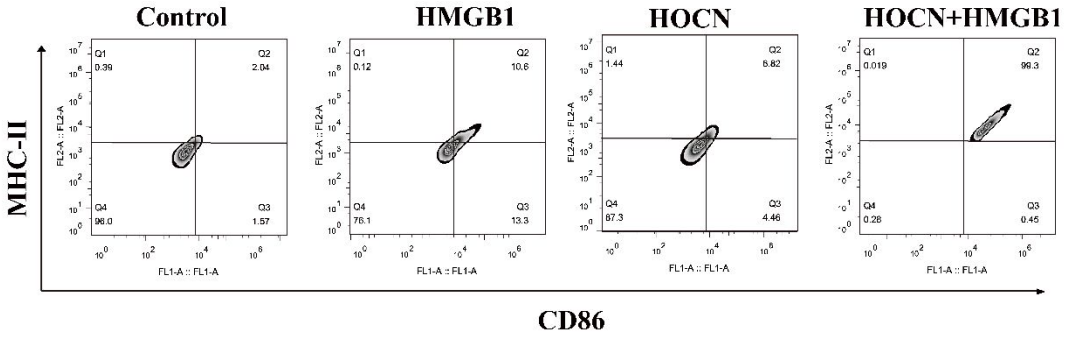

Fig.S9 Flow cytometry analysis of co-stimulatory molecules CD86 and MHC II complexes expression in DCs with different treatments for 24 h.

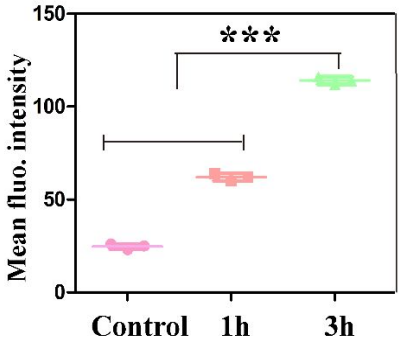

Fig. S10 Mean fluorescence intensity (MFI) of intracellular Ca^{2+} level in CT26 cells. Results are presented as means ± s.d., n=4, *$P < 0.05$, **$P < 0.01$, and ***$P < 0.001$ determined by Student's t test.

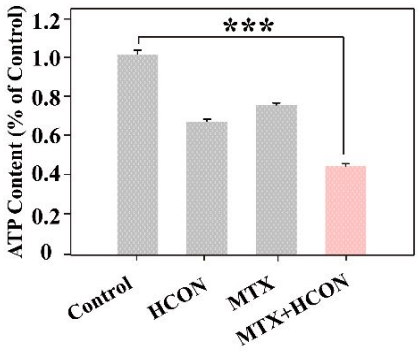

Fig. S11 The intracellular ATP content of CT26 cells treated with HOCN, MTX and MTX+HOCN for 4 h (equivalent MTX: 20 nM, HOCN: 40 μg/mL). Results are presented as means ± s.d., n=4, **P* < 0.05, ***P* < 0.01, and ****P* < 0.001 determined by Student's t test.

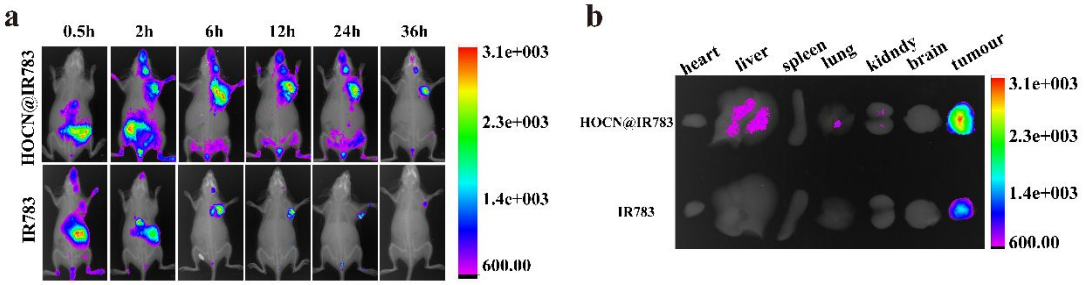

Fig. S12 Optical imaging of CT26 tumor-bearing mice (A) and the main tissues (B) after injection of IR783 and HOCN@IR783 (with the same dosage of IR783) for different time periods.

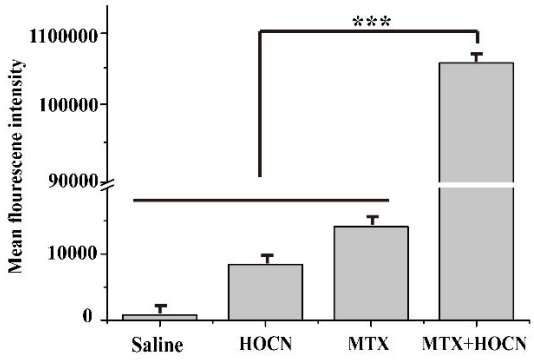

Fig. S13 Mean fluorescence intensity (MFI) of tunel level in tumor section. Results are presented as means ± s.d., n=5, **P* < 0.05, ***P* < 0.01, and ****P* < 0.001 determined by Student's t test.

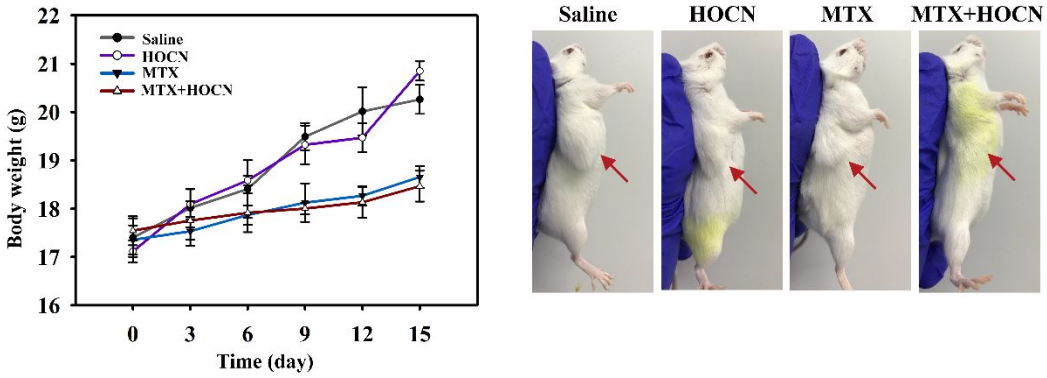

Fig. S14 (A) The body weight change curves of CT26 tumor-bearing mice during treatment with different formulations; (B) Representative photos of CT26 tumor-bearing mice after receiving different treatments, red arrow points tumors. Results are presented as means ± s.d., n=5.

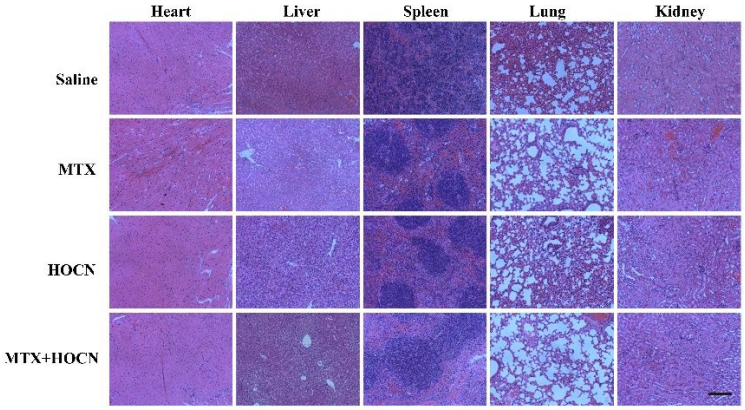

Fig. S15 Hematoxylin-eosin (H&E) analysis of heart, liver, spleen, lung and kidney from CT26 tumor-bearing mice after receiving different treatments for 15 d, scale bar: 200 μm.

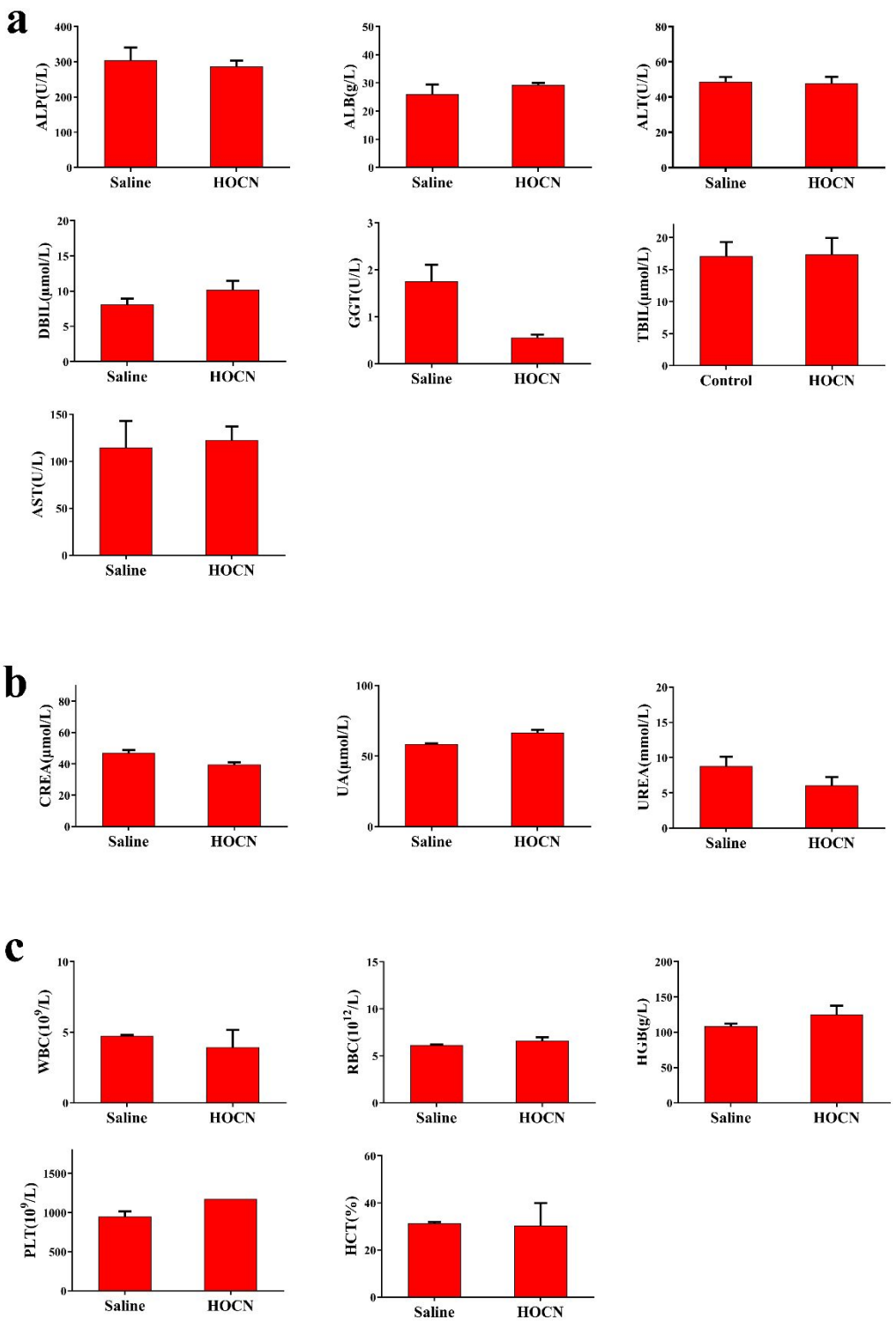

Fig. S16 Major liver function indexes (a), kidney function indexes (b) and blood routine indexes (c) of mice in different treatment group, n=5.

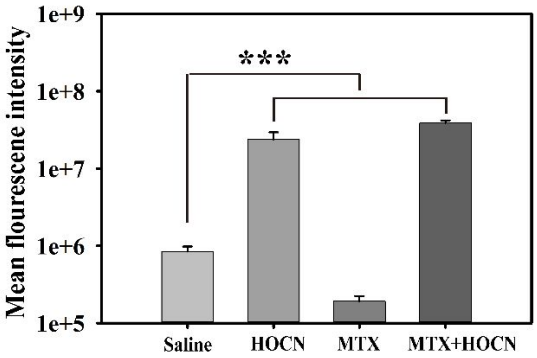

Fig. S17 Mean fluorescence intensity (MFI) of LC3-II level in tumor lymph nodes. Results are presented as means ± s.d., n=5, **P* < 0.05, ***P* < 0.01, and ****P* < 0.001 determined by Student's t test.

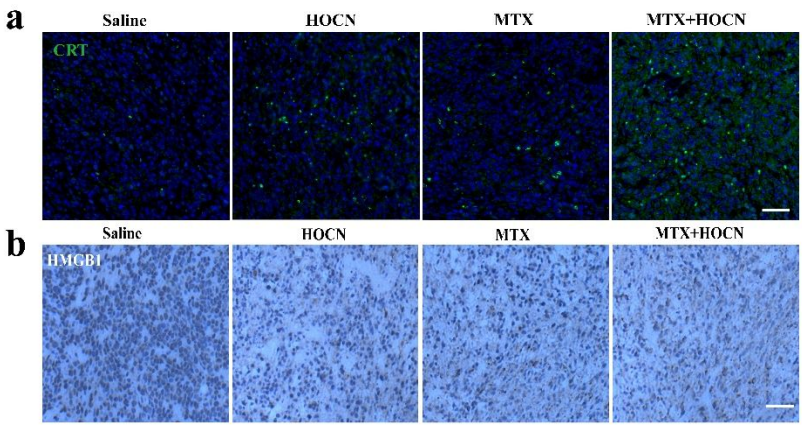

Fig. S18 HOCN efficiently enhanced DAMPs release from CT26 cells *in vivo*. (A) CRT exposure in tumor tissue from CT26 tumor-bearing mice after receiving different treatments, scale bar: 100 μm; (B) HMGB1 release from CT26 cells in tumor tissue from CT26 tumor-bearing mice after receiving different treatments, scale bar: 100 μm.

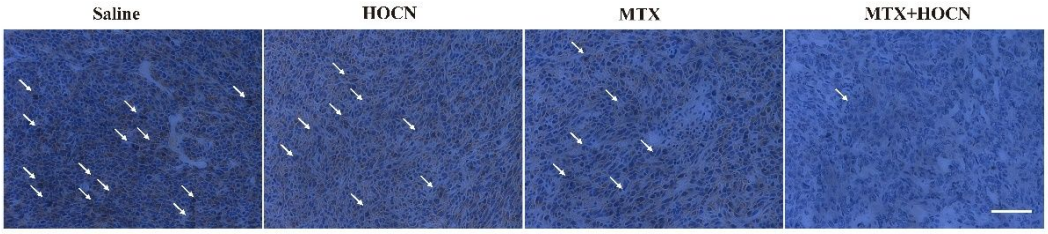

Fig. S19. Representative Immunohistochemistry images of TGF-β in tumor from each group, the white arrow shows TGF-β, scale bar: 100μm;

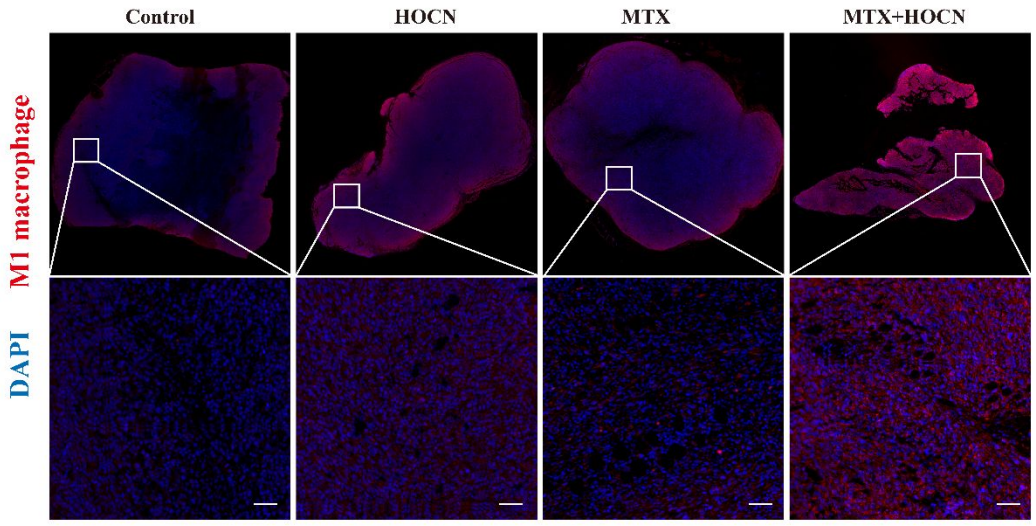

Fig.S20 Representative immunofluorescence images of M1 macrophage infiltration in tumor from each group scale bar: 50μm;

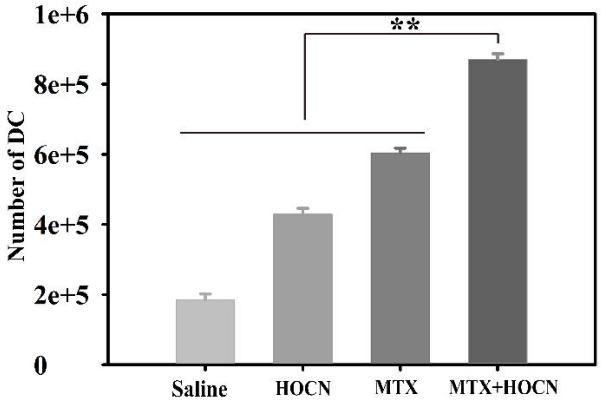

Fig. S21 Numbers of DCs in tumor lymph nodes from CT26 tumor-bearing mice after receiving different treatments for 10 d (3 round treatments). Results are presented as means ± s.d., n=5, **P* < 0.05, ***P* < 0.01, and ****P* < 0.001 determined by Student's t test.

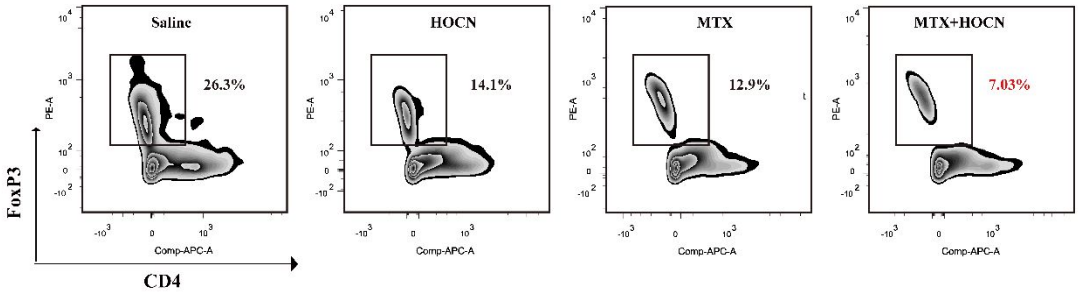

Fig. S22 Flow cytometric analysis of FoxP3^{+} CD4^{+} T lymphacytes in CT26 tumor-bearing mice receiving different treatments (gated on CD3^{+}).

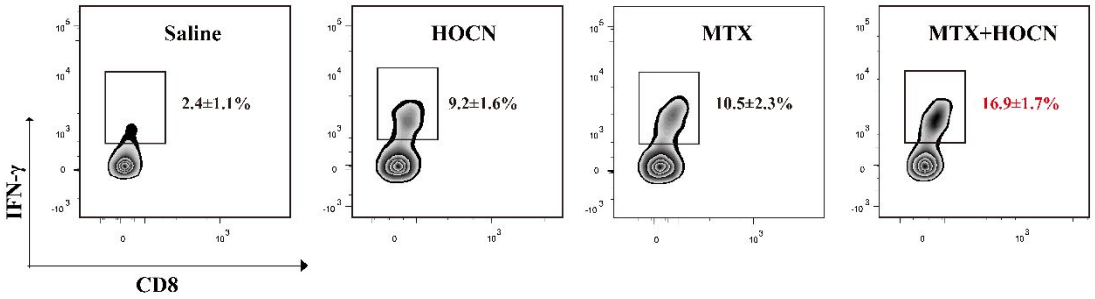

Fig. S23 Flow cytometric analysis of IFN-γ^+ $CD8^+$ T lymphacytes in CT26 tumor-bearing mice receiving different treatments (gated on $CD3^+$). Results are presented as means ± s.d., n=5.

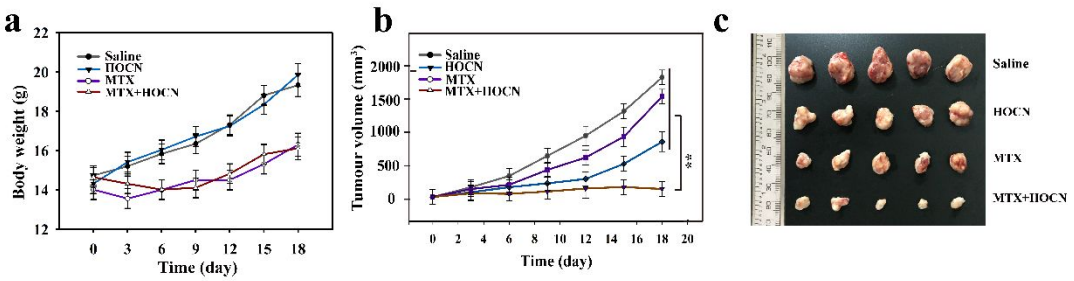

Fig. S24 HOCN enhanced MTX-mediated chemo-immunotherapy in CT26 tumor-bearing distant tumor model. (A) The body weight change curves of CT26 tumor-bearing distant tumor model during treatment with different formulations; (B) The growth curves and (C) representative tumor images of primary tumor from each group. Results are presented as means ± s.d., n=5, *$P < 0.05$, **$P < 0.01$, and ***$P < 0.001$ determined by Student's t test.